Research Article Vol. 32, No. 23 / 4 Nov 2024 / Optics Express 40326
Optics EXPRESS

Reservoir computing for equalization in a self-coherent receiver scheme

AIMEN ZELACI,[1,*] SARAH MASAAD,[2] AND PETER BIENSTMAN[2]

[1]IDLab, Department of Information Technology Ghent University - imec, Belgium
[2]Photonics Research Group, Department of Information Technology, Ghent University - imec, Belgium
[*]aimen.zelaci@imec.be

Abstract: Short-reach optical networks, the backbone of data centers, face a significant challenge: transmitting high data rates at low cost and low energy consumption. While coherent signals can carry high data rates, coherent receivers are expensive and complex. Also, to equalize channel dispersion, they rely on digital signal processing modules, which consume large amounts of power and introduce more latency. Photonic reservoirs emerged as a way to process these signals in the analog optical domain, alleviating the power consumption and latency issues in state-of-the-art receivers. In this work, we show in simulations that a photonic reservoir combined with a self-coherent photonic receiver achieves a BER of 3.8×10^{-3} for a 32 Gbaud 16-QAM signal and an 80 km link, requiring a low CSPR of 3 dB compared to state-of-the-art self-coherent receivers.

1. Introduction

Optical fibers orchestrate communications inside and between data centers. These centers house vital modern-day services, from social media servers and servers processing data from Internet of Things (IoT) devices to cloud and hyper-scale artificial intelligence (AI) computing. Internet users grew from 3.9 billion in 2018 to 5.18 billion in 2023, which is 64.6% of the world's population [1]. The number of connected devices twice surpassed the global population (15.14 billion) as of April 2023. Data centers require low-cost and power-efficient short-reach optical networks to move this sheer amount of data at high bit rates.

Short-reach optical networks range from a few meters inside a data center to about 120 km between data centers. Traditional short-reach networks directly detect intensity-modulated (IM) signals using a single photodiode. Indeed, direct detection (DD) offers an efficient solution for these short-reach communications. Even though IM-DD systems represent an attractive solution, fiber impairments like chromatic dispersion limit the transmission reach to under 10 km [2]. These rates appear minuscule compared to those achieved by coherent signals typically transmitted over long-haul links.

Coherent signals encode data in both the intensity and phase of a signal. They accelerated the capacity growth of optical links to the Tb/s regime for long-haul communications systems [3]. Current coherent detection systems include advanced digital processing (DSP) modules and several expensive high-speed components. Thus, coherent detectors are undesirable for short-reach links. This motivated the idea of pioneering "self-coherent" DD systems as an efficient way to reconstruct coherent signals in short-reach networks.

Self-coherent systems use a single photodiode and a dedicated algorithm to extract phase and amplitude information [2]. When viewed in the frequency domain, a self-coherent signal incorporates the main message and a strong DC subcarrier. The power ratio of the DC subcarrier to that of the main message is referred to as the carrier-to-signal power ratio (CSPR). A popular self-coherent receiver is the Kramers-Kroning (KK) DSP receiver [4]. A study in [5] demonstrated that a KK receiver achieves 400 Gb/s for a distance of 80 km at a CSPR of 15 dB. Alternative detection techniques, such as carrier-assisted differential detection (CADD) [6] and asymmetric

#534576 https://doi.org/10.1364/OE.534576
Journal © 2024 Received 2 Jul 2024; revised 30 Sep 2024; accepted 8 Oct 2024; published 22 Oct 2024

Optics EXPRESS

self-coherent detection (ASCD) [7], have been proposed to replace self-coherent signaling, requiring CSPR values of around 13 dB. Unfortunately, such receivers suffer from two main problems: (1) high CSPR values (or high power consumption), and (2) complicated signal equalization using DSP modules. These are the main problems that we wish to alleviate.

DSP chips draw considerable power, especially when processing fast signals [8,9]. Additionally, the processing run time of DSP units raises latency concerns. A possible solution would be processing signals (possibly partly) in the analog optical domain, as this can improve power consumption and processing delays. Advances in photonic integrated circuits (PICs) paved the way for new interesting optical signal processors, e.g. based on artificial neural networks and related concepts like reservoir computing.

Artificial neural networks (ANNs) can solve problems that traditional computer algorithms struggle to solve, like image recognition or text processing and generation. While most ANNs have a so-called feedforward structure, some architectures incorporate feedback loops to realize memory. These so-called recurrent neural networks (RNNs), were initially difficult to train, which prompted researchers to propose the reservoir computing (RC) paradigm [10], [11], [12] which consists of a randomly initialized fixed RNN followed by a trainable linear readout. These architectures are well-suited to be implemented in silicon photonics.

Past studies [13–17] used photonic reservoirs to solve problems such as a temporal XOR task with memory, header recognition, and dispersion compensation for 32 Gbps *on-off-keying* (OOK) signals. A more recent study demonstrated that a reservoir can equalize link nonlinearities for a 64-QAM signal using a KK receiver [18]. The work in [19] introduced a new photonic reservoir architecture called the Recurrent Optical Spectrum Slicing Neural Networks (ROSS-NNs) and demonstrated that this reservoir can equalize 120 Gbaud 16-QAM and 32-QAM signals at 20 km and 5 km respectively for the same CSPR values as a KK receiver. This paper on the other hand studies a new system with a photonic linearizer instead. The paper's novelty lies in constructing a photonic system for the direct detection and equalization of coherent signals. To the best of our knowledge, there has been no study yet for such a system.

2. Goals and structure

This paper studies a photonic system that detects and equalizes self-coherent signals with low CSPR values using a photonic reservoir as the main equalization block. The receiver is the integrated photonic self-coherent receiver developed in [20], which operates mainly in the analog domain and requires CSPR values of 0 to 5 dB.

The rest of this paper is structured as follows. Section 3 discusses the self-coherent receiver used in this work. Section 4 presents the architecture of the photonic reservoir and design considerations. Section 5 presents the simulation setup, whose results are presented in Section 6. Finally, Section 7 summarizes the main results of this work and presents future outlooks.

3. Self-coherent receiver

A conventional coherent receiver recovers the amplitude and phase of a coherent signal using a local oscillator and several mixers and detectors. Alternatively, only a single photodetector can recover a coherent signal, provided we use a so-called self-coherent signal.

A self-coherent signal contains an additional subcarrier to, for example, the left of the baseband message signal (Fig. 1). The ratio of the subcarrier power to the baseband signal is called the carrier-to-signal power ratio (CSPR). Finally, the distance in Hertz between the subcarrier and the baseband message is called the guardband.

Consider a receiver with only a single photodetector, and a self-coherent signal $S+m$ impinging on it where m is the complex-valued coherent message signal and S is the subcarrier, which is assumed to be real-valued, without loss of generality. Upon reception, this subcarrier is

Optics EXPRESS

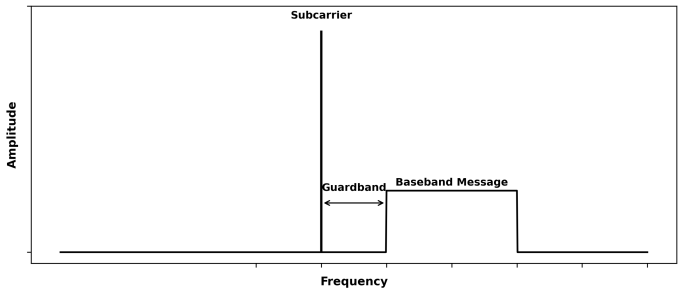

Fig. 1. The frequency content of a self-coherent signal.

positioned at DC. The photodetector outputs the modulus squared of the input signal:

$$|S+m|^2 = (S+m)(S+m^*) = S^2 + Sm + Sm^* + mm^* \tag{1}$$

The first term is a DC component. The second term is a linear replica of the message. The third term is a replica of the complex conjugate of the message, which can be filtered out. However, the last term represents a nonlinear component that resides on top of the baseband in the frequency domain. This term is also known as the signal-to-signal beat interference (SSBI) term. One way to handle this is by having a large CSPR, such that the linear replica of the message dominates the detected signal. The value of the required CSPR depends on the receiver's topology. Researchers developed new receivers that require smaller CSPR values. One common receiver is the Kramers-Kronig receiver which requires a value of $\sim 11-15\ dB$ [4,5,18], as well as a DSP module to process and linearize the signal.

Alternatively, Lyu *et al.* [20] proposed linearizing the signal in the analog photonic domain using a silicon photonics circuit. The photonic linearizer uses two photodiodes and requires CSPR values of only $0-5\ dB$. The circuit consists of a splitter and two waveguide branches, as shown in Fig. 2. Assuming the splitter, ring resonator, and photodiodes are ideal, the output after each stage is as follows:

$$\begin{aligned} \text{The input:} \quad & S+m \\ \text{The 3 dB splitter:} \quad & \frac{1}{\sqrt{2}}(S+m) \\ \text{The ring resonator:} \quad & \frac{1}{\sqrt{2}}m \\ \text{The output:} \quad & \frac{1}{2}\left(S^2 + Sm + Sm^*\right) \end{aligned} \tag{2}$$

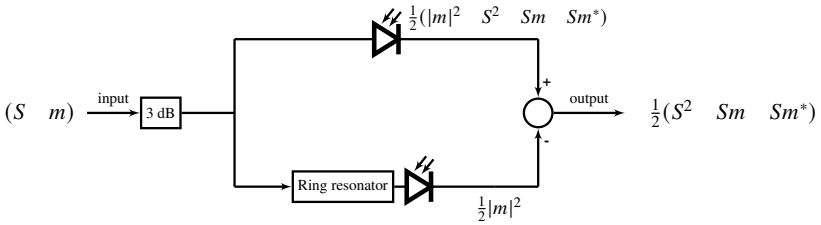

Fig. 2. Diagram of the photonic linearizer annotated with corresponding equations.

Optics EXPRESS

The ring resonator in the bottom arm filters out the subcarrier. By subtracting the signals from the two arms, the SSBI term is eliminated. The signal is free of nonlinear distortion if the circuit is ideal, i.e., if the arms are matched and the ring has an infinite extinction ratio.

This subtraction happens in the digital electronic domain. This means that two analog-to-digital converters (ADC) must be added to the top and bottom arms of the photonic linearizer. Additional DSP follows the subtraction to recover the transmitted coherent signal (Fig. 3). The DSP blocks used here do not handle signal distortion, which we wish to handle in the optical domain using reservoir computing (RC).

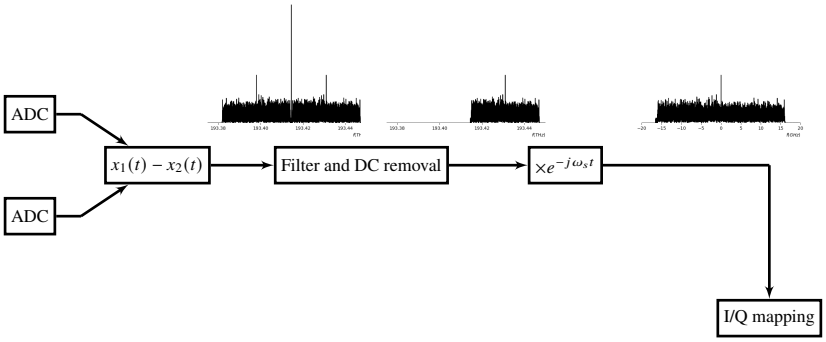

Fig. 3. Signal recovery in the electronic domain.

4. Photonic reservoir

RC was introduced to simplify the training of recurrent neural networks (RNNs). Rather than training all the weights inside a recurrent network, they are randomly initialized and fixed. What is trained, however, is a simple linear readout layer (Fig. 4), that takes linear combinations of the states inside the network. This is essentially linear regression, which is much easier to perform.

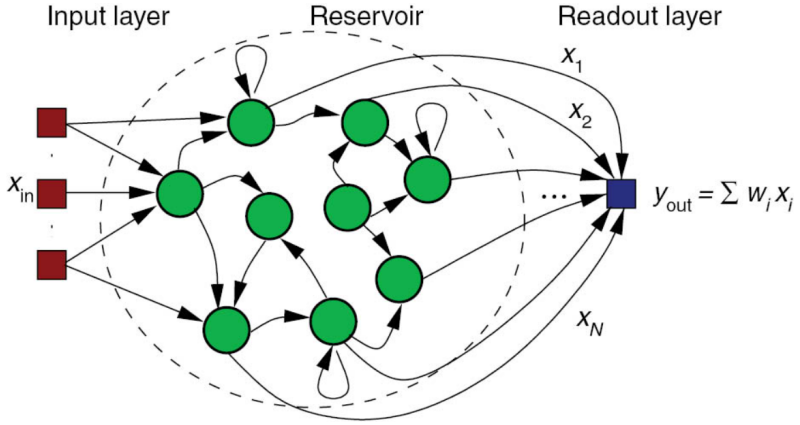

Fig. 4. Reservoir schematic [*Van der Sande, G., Brunner, D., Soriano, M. C. (2017). Advances in photonic reservoir computing. Nanophotonics, 6(3), 561-576.*]

The reservoir can be implemented in photonics hardware, using a variety of approaches (see [21]). In this work, we consider a space-multiplexed reservoir with a four-port architecture (Fig. 5), which was experimentally demonstrated in [16] in an integrated photonics chip. In this architecture, the nodes are multimode interferometers (MMIs) interconnected by spiral

Optics EXPRESS

waveguides. An interconnection delay of half the bit rate ensures that ISI cancellation occurs at the sampling midpoint. This is not always the optimum strategy, but from our previous work [18] we demonstrate optimization results that show that half the bit rate is the optimum interconnection delay. The output layer is a so-called optical readout where complex-valued optical weights modulate the different output channels of the reservoir, and they are subsequently combined in a single photodiode [22].

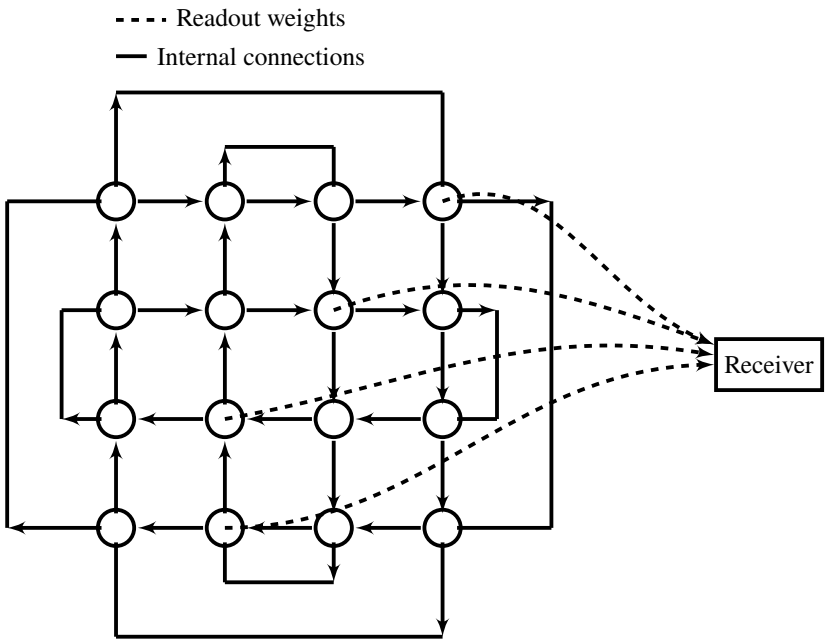

Fig. 5. Space-multiplexed reservoir with a four-port architecture.

Training the reservoir boils down to finding the weights of the linear readout layer. For a given complex-valued target, a closed-form solution exists, using linear regression and the Moore-Penrose pseudo-inverse:

$$W = (\tilde{X}^{\dagger}\tilde{X} + \lambda I)^{-1} X^{\dagger}\tilde{Y} \tag{3}$$

Here, $\tilde{X}$ is the input vector to the readout and $\tilde{Y}$ is the output target vector (after the receiver), W is the weight vector, λ is a regularization parameter, and I is the identity matrix.

In our case, it is difficult to define a complex-valued optical target before the receiver, i.e. just after the linear combination. This is because the signal before the receiver could be very different from the one after it, because of nonlinearities and imperfections. Therefore, we decided to model the receiver completely and include it in the weight optimization pipeline. However, this means we can no longer use linear regression but need to rely on backpropagation instead.

Backpropagation consists of defining a cost function of the weights, the mean squared error for example, and using a dedicated algorithm, such as stochastic gradient descent (SGD), to find the weights that minimize the cost function by propagating it back through the network for some training epochs. However, we still need a good initial guess for gradient descent to converge efficiently to a better minimum than if the weights are randomly initialized. For that purpose, we constructed a first set of weights that assumes an ideal linear receiver, such that we can use Eq. (3).

Optics EXPRESS

5. Simulation setup

The transmitter and fiber link were simulated using VPItransmissionMaker [23]. Figures 6 and 7 demonstrate the simulation setup. The link contains a standard single-mode fiber (SMF) loop with an erbium-doped amplifier (EDFA). Table 1 summarizes the parameters of the link; we believe that 32 Gbaud 16-QAM is a good starting point to study the new receiver. The optical reservoir and linearization chip were simulated using Photontorch [24]. Table 2 contains the reservoir and training parameters. The reservoir is trained multiple times on different runs with random waveguide phases to evaluate process variations. Further DSP functions at the receiver were implemented using Python.

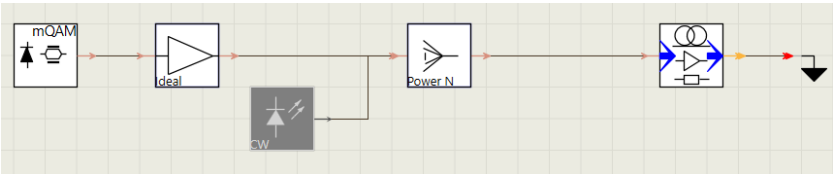

Fig. 6. System that generates a target signal.

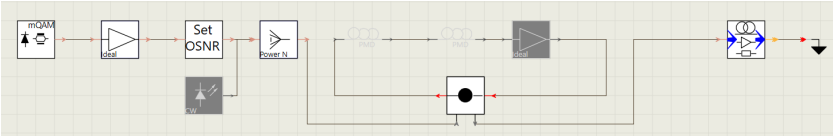

Fig. 7. System that generates the output signal of a fiber channel.

Table 1. Link parameters. RRC: Root-raised cosine filter which is matched at the receiver's end.

Parameter	Value
Fiber length	20 km to 100 km
Symbol rate	32 Gbaud
Bits per symbol	4 (16-QAM)
Samples per symbol	16
Carrier frequency	193.41 THz
Laser power	3 dBm
Nyquist filter	RRC
Filter roll-off	0.01
Code	Gray
FEC limit	3.8×10^{-3}
Dispersion parameter	$17 ps/km/nm$
Fiber non-linearity index	$2.6 \times 10^{-20} um^2 \cdot W^{-1}$
OSNR	25 dB

Optics EXPRESS

Table 2. Reservoir parameters. The effective index is of a silicon nitride platform.

Parameter	Value
Nodes	4×4
Interconnection delay	$\frac{0.5}{Symbol\ rate}$ s
Effective refractive index n_{eff}	1.7587
Group index (n_g)	2.117
Waveguide loss	25 dB/m
MMI loss	1 dB
Cost function	Mean-squared error (MSE)
Performance metric	BER
Training optimizer	SGD with momentum [25]
Training epochs	500
Training set size	16×2^{13}
Testing set size	16×2^{13}

6. System study

To study the full link, we adopt a progressive strategy. First, we focus on understanding the linearization chip by simulating a back-to-back system that contains only the transmitter and the receiver. Second, we analyze the full link with the reservoir and investigate the equalization performance.

6.1. Analysis of the linearization chip

The heart of the linearization chip is a ring resonator. However, the nonidealities of the ring allow for a fraction of the nonlinear distortion to survive after the subtraction stage. These nonidealities arise due to propagation and coupling losses that reduce the ring's Q-factor and extinction ratio. Additionally, process variations alter the effective refractive index, causing the resonance wavelength to shift from the subcarrier. To help visualize these effects, we plotted in Fig. 8 a view of the self-coherent signal with the ring's response.

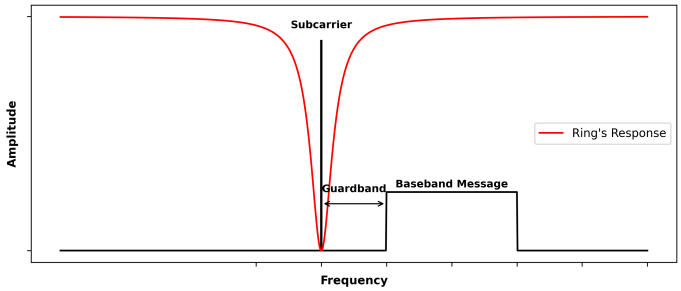

Fig. 8. The frequency content of a self-coherent signal with the ring's response.

To quantify the nonidealities mentioned above, we simulated a back-to-back system for different values of the Q-factor of the ring and of the CSPR values for a varying frequency offset of the ring's resonance. The target resonance frequency is positioned at the subcarrier frequency located at the edge of a 2 GHz guardband away from the message.

First, the CSPR was fixed at 3 dB and the Q-factor was varied. Simulation results in Fig. 9 indicate that when |offset|>20 GHz, the resonance of the ring is so far removed from the frequency

Optics EXPRESS

range of the message, that the signals from both arms become equal, attenuating the entire signal after subtraction. As the resonance moves toward the subcarrier, the BER drops to a minimum at an offset of 0.25 GHz for every Q-factor. The minimum value of the BER increases beyond the FEC limit when the Q-factor becomes too small, as the ring starts to attenuate more parts of the baseband message. For $Q = 1342$, the dip in the BER curve begins to vanish because, at this point, the Q-factor is so small that the ring hardly functions as a filter anymore, when this signal is subtracted from the upper arm's signal, most of the nonlinear term survives.

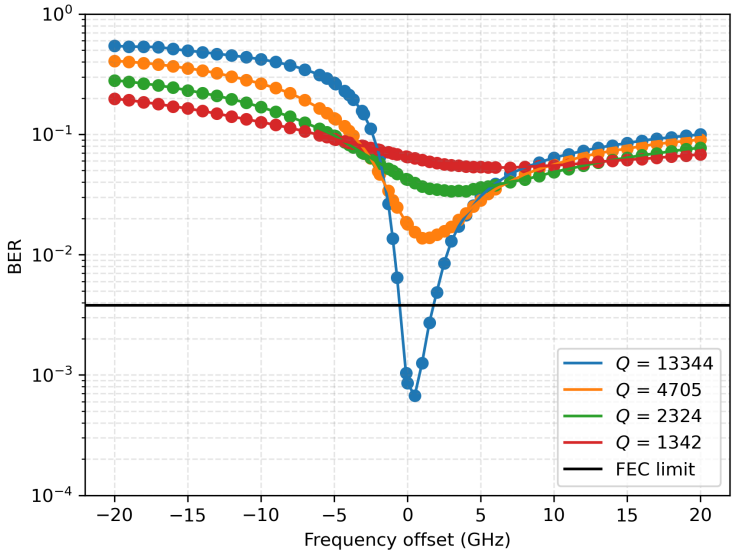

Fig. 9. The BER versus the resonance offset of the ring for different Q-factors, CSPR = 3 dB. The resonance is to the left of the subcarrier for a positive offset, and to the right for a negative offset.

Second, the Q-factor was fixed at 13344 and the CSPR was varied. As mentioned before, for higher CSPR, we expect performance to improve, as the relative influence of the nonlinear term at the detector decreases compared to the linear replicas of the message signal. Results in Fig. 10 confirm that high CSPR values indeed reduce the BER to 0.0 for a CSPR value of 5 dB.

6.2. Analysis of the complete link

A signal experiences several distortions after propagating through an optical link. These impairments stem from different parts of the link. We can summarize them as follows: (1) Noise, such as the spontaneous emission noise of optical amplifiers (2) Dispersion due to the nonlinear Kerr effect, which we shall call Kerr dispersion for brevity, (3) The receiver's nonlinearity, and (4) chromatic dispersion. Our goal is to train the photonic reservoir to handle Kerr dispersion, the receiver's nonlinearities, and chromatic dispersion.

This part studies the equalization of system impairments by looking into two different variants of the link: (1) a system that includes an ideal dispersion-compensating fiber (DCF) that insulates the system from chromatic dispersion, and (2) a system that excludes the DCF, forcing the reservoir to compensate for both nonlinear effects and chromatic dispersion.

6.2.1. Only nonlinear effects compensation

Figure 11 depicts the system studied in this part. The SMF has a length of 100 km. The amplifier is an erbium-doped fiber (EDFA). The reservoir is trained to compensate for the Kerr dispersion

Optics EXPRESS

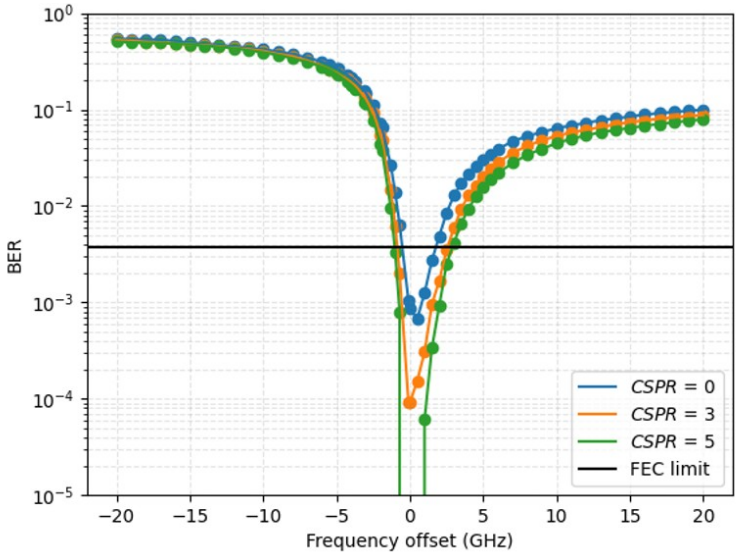

Fig. 10. The BER versus the CSPR for a back-to-back system. Q = 13344.

and the receiver's nonlinearity. We also simulated a system with an ideal bandpass filter instead of the reservoir for benchmarking. The considered ideal bandpass filter has a rectangular shape in the frequency domain.

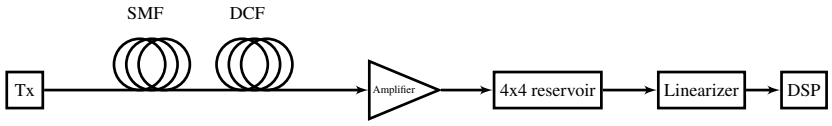

Fig. 11. System for nonlinear effects compensation.

First, the size of the guardband and the ring's resonance were fixed. The system was simulated for a varying CSPR. The results in Fig. 12 show that the reservoir reduces the BER by an order of magnitude, as it equalizes for Kerr dispersion, and learns to mitigate SSBI through backpropagation. For the simulated CSPR range, and given the resolution limit of the BER, the low BER is more or less unaffected by the CSPR for both systems. The reservoir system experiences larger BER variations for larger guardbands (Also refer to Fig. 14) because the noise just outside the baseband message can distort the signal after downsampling, affecting the initial weights found through linear regression.

Second, the guardband was fixed at 0.5 GHz and the resonance offset with respect to the subcarrier frequency was swept. The results in Fig. 13 demonstrate that a minimum occurs near an offset of 0.25 GHz for both systems instead of 0 GHz because the notch filter has a finite Q-factor. As a result, it attenuates parts of the message when it is closer to it. The reservoir allows for a displacement of ~ 0.75 GHz in the negative direction and ~ 1.25 GHz in the positive direction with respect to this minimum. The allowed displacements for the system without the reservoir are ~ 0.25 GHz and ~ 0.5 GHz respectively. Therefore, the reservoir tolerates larger values of resonance displacement because the reservoir learns the imperfections of the receiver through backpropagation.

Finally, we swept the guardband size, with the ring's resonance aligned with the subcarrier. For brevity, only the system with a 4x4 reservoir was simulated, as the previous results clearly

Optics EXPRESS

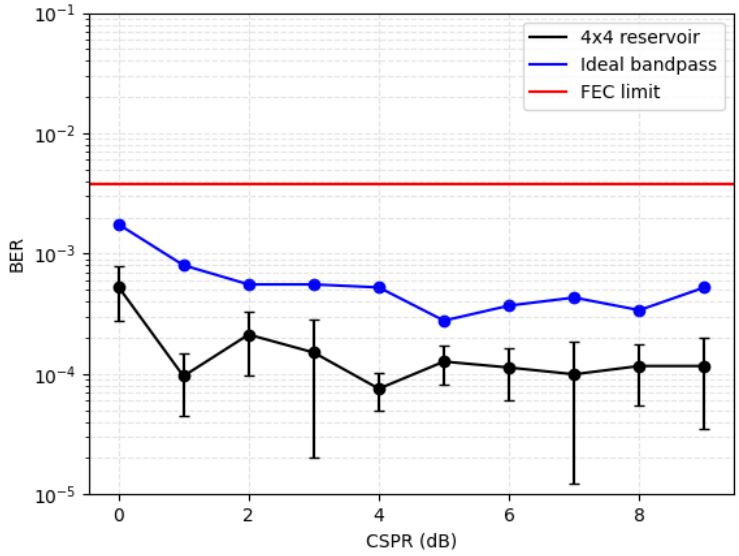

Fig. 12. BER versus CSPR for the system in Fig. 11. The guardband = 2 GHz, Q = 13344. The ring's resonance is located at the subcarrier frequency.

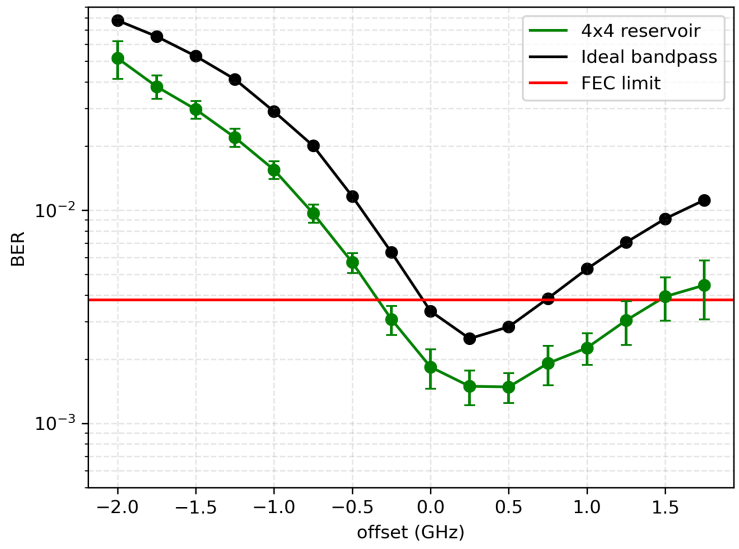

Fig. 13. BER versus the offset of the ring's resonance for the link of Fig. 12, and the same link but with an ideal bandpass filter instead of the reservoir. Q = 13344, CSPR = 3 dB. Guardband = 0.5 GHz.

Optics EXPRESS

show the advantages of the reservoir. The results in Fig. 14 demonstrate a trade-off between spectral efficiency and CSPR: for higher spectral efficiency (i.e. smaller guard band), the system needs a higher CSPR to remain below the FEC limit. For example, for a 0 GHz guardband, 6 dB CSPR is needed, but this is reduced to 0 dB for a guardband of 1 GHz.

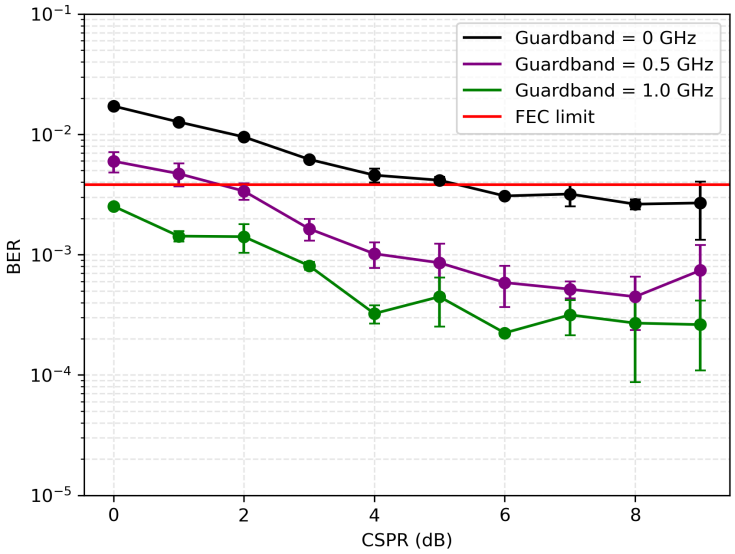

Fig. 14. BER versus CSPR for the reservoir system in Fig. 11 for different guardbands.

6.2.2. Both chromatic and Kerr dispersion compensation

As mentioned in the earlier sections, we aim to study the performance of the reservoir in compensating for fiber dispersion and the receiver's imperfections. In the link studied in this part, shown in Fig. 15, a bandpass filter allows the reservoir to focus mainly on dispersion by diminishing the effects of the link's noise. We choose the coupled-resonator optical-waveguide circuit (CROW) for the bandpass filter in this work. Table 3 summarizes the simulation parameters for this particular link.

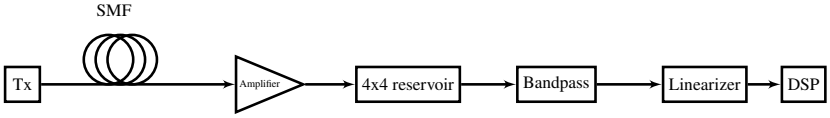

Fig. 15. System for linear and Kerr dispersion compensation.

The results of Fig. 16 indicate that a 4x4 reservoir compensates for chromatic dispersion up to 80 km, where the reservoir runs out of memory to deal with the accumulated dispersion. The distortions imposed by the CROW appear limited, as it results in a BER close to that of an ideal bandpass filter. As for the distortions of the receiver's ring, Fig. 17 shows that the reservoir maintains a low BER until 60 km, even for the lowest Q-factor considered.

In our final simulations, we compared the performance of the reservoir to that of an electronic tapped delay line (TDL). The TDL operates in the digital domain and equalizes for chromatic dispersion after the receiver distorts the signal; that is, the TDL performs post-compensation. The weights of the TDL are calculated using the linear regression of Eq. (3) without the need for backpropagation.

Optics EXPRESS

Table 3. Simulation parameters of the system in Fig. 15.

Parameter	Value
CSPR	3 dB
Guardband	0.5 GHz
Length of the SMF	Varied from 20 km in steps of 20 km
Resonance offset of ring	0.25 GHz
Q-factor of the receiver's ring	13344
number of rings in CROW	11

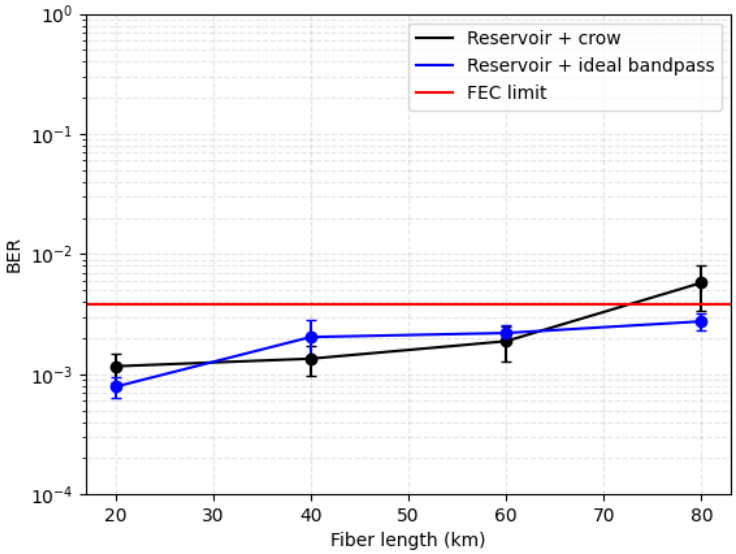

Fig. 16. BER of the link in Fig. 15. The parameters are shown in Table 3.

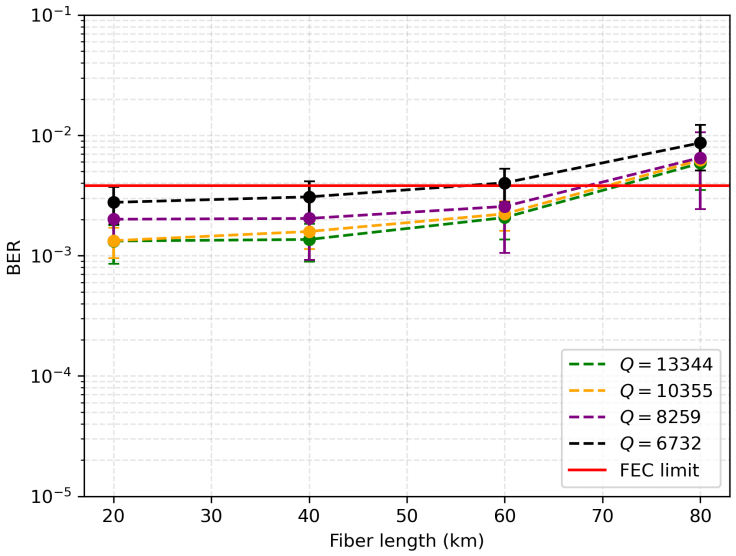

Fig. 17. Performance of the reservoir of the link in Fig. 15 for different Q-factors of the receiver's ring. The rest of the parameters are shown in Table 3

Optics EXPRESS

The results in Fig. 18 show that the reservoir outperforms the TDL for lengths up to 80 km. The simulation parameters are the same as in Table 3, except for the Q-factor of the receiver's ring which was set to 6732, i.e. the worst case of the results in Fig. 17.

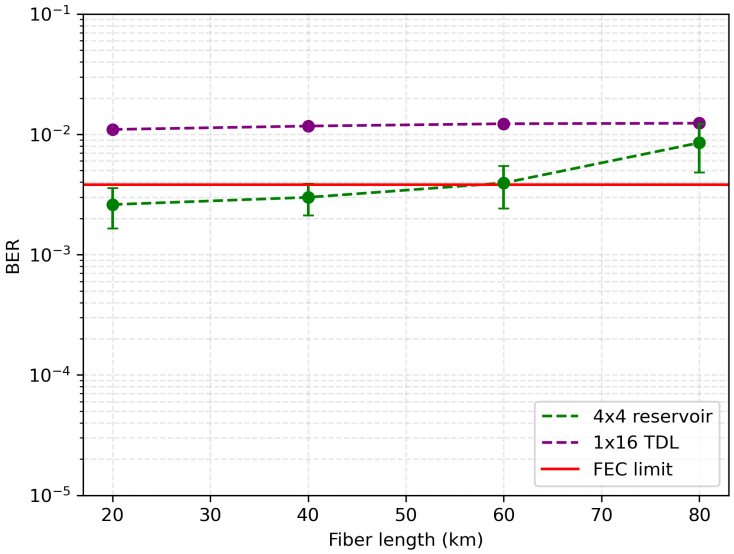

Fig. 18. Performance of a 4x4 reservoir compared to a 1x16-TDL.

The photonic reservoir equalizes chromatic dispersion in real-time in the analog photonic domain. Thus, we can intuitively predict significant improvements in complexity, power, and latency compared to an electronic digital equalizer. A quantitative analysis is left for future work.

7. Conclusion

Self-coherent direct detection systems emerged to efficiently transmit coherent signals in short links. In this work, we investigate a self-coherent DD system using a photonic circuit that combines a 4x4 photonic reservoir and a bandpass filter. This system achieved BER values below the FEC limit of 3.8×10^{-3} for links up to 80 km and a 16-QAM 32 Gbaud signal at a CSPR value of 3 dB. The reservoir was shown to outperform an electronic chromatic dispersion compensator because it pre-compensates the dispersion before the receiver distorts the signal. The reservoir exploits backpropagation to mitigate any residual SSBI of the receiver.

Future work will focus on the experimental realization of this receiver and higher-order QAM formats. Indeed, for 64-QAM or 256-QAM, the symbols come close together in the constellation diagram, which sets more stringent requirements for the system.

Funding. Horizon 2020 Framework Programme (GA101070195, GA860360, GA871330, GA871658); Fonds Wetenschappelijk Onderzoek (G006020N).

Disclosures. The authors declare no conflict of interest.

Data availability. Results data presented in this study can be accessed upon reasonable request.

References

1. C. Systems, "Annual internet report," (2023). Accessed: June 6, 2023.
2. X. Chen, C. Antonelli, A. Mecozzi, *et al.*, "High-capacity direct-detection systems," in *Optical Fiber Telecommunications VII*, (Elsevier, 2020), pp. 419–441.
3. E. Agrell, M. Karlsson, A. Chraplyvy, *et al.*, "Roadmap of optical communications," J. Opt. **18**(6), 063002 (2016).
4. A. Mecozzi, C. Antonelli, and M. Shtaif, "Kramers–kronig coherent receiver," Optica **3**(11), 1220–1227 (2016).

Optics EXPRESS

5. S. T. Le, K. Schuh, R. Dischler, *et al.*, "Beyond 400 gb/s direct detection over 80 km for data center interconnect applications," J. Lightwave Technol. **38**(2), 538–545 (2020).
6. J. Li, Z. Wang, H. Ji, *et al.*, "High electrical spectral efficiency silicon photonic receiver with carrier-assisted differential detection," in *Optical Fiber Communication Conference*, (Optica Publishing Group, 2022), pp. Th4B–6.
7. Y. Hu, X. Li, D. Mao, *et al.*, "Transmission of net 200 gbps/λ over 40 km of smf using an integrated sip phase-diverse receiver," in *European Conference and Exhibition on Optical Communication*, (Optica Publishing Group, 2022), pp. Th3B–6.
8. J. C. Cartledge, F. P. Guiomar, F. R. Kschischang, *et al.*, "Digital signal processing for fiber nonlinearities," Opt. Express **25**(3), 1916–1936 (2017).
9. I. A. Young, E. Mohammed, J. T. Liao, *et al.*, "Optical i/o technology for tera-scale computing," IEEE J. Solid-State Circuits **45**(1), 235–248 (2009).
10. H. Jaeger, "The 'echo state' approach to analysing and training recurrent neural networks-with an erratum note," Bonn, Germany: German National Research Center for Information Technology GMD Technical Report **148**, 13 (2001).
11. W. Maass, T. Natschläger, and H. Markram, "Real-time computing without stable states: A new framework for neural computation based on perturbations," Neural Computation **14**(11), 2531–2560 (2002).
12. D. Verstraeten, B. Schrauwen, M. D'Haene, *et al.*, "An experimental unification of reservoir computing methods," Neural Networks **20**(3), 391–403 (2007).
13. K. Vandoorne, W. Dierckx, B. Schrauwen, *et al.*, "Toward optical signal processing using photonic reservoir computing," Opt. Express **16**(15), 11182–11192 (2008).
14. K. Vandoorne, P. Mechet, T. Van Vaerenbergh, *et al.*, "Experimental demonstration of reservoir computing on a silicon photonics chip," Nat. Commun. **5**(1), 3541 (2014).
15. A. Argyris, J. Bueno, and I. Fischer, "Photonic machine learning implementation for signal recovery in optical communications," Sci. Rep. **8**(1), 8487 (2018).
16. S. Sackesyn, C. Ma, J. Dambre, *et al.*, "Experimental realization of integrated photonic reservoir computing for nonlinear fiber distortion compensation," Opt. Express **29**(20), 30991–30997 (2021).
17. M. Sorokina, S. Sergeyev, and S. Turitsyn, "Fiber echo state network analogue for high-bandwidth dual-quadrature signal processing," Opt. Express **27**(3), 2387–2395 (2019).
18. S. Masaad, E. Gooskens, S. Sackesyn, *et al.*, "Photonic reservoir computing for nonlinear equalization of 64-qam signals with a kramers–kronig receiver," Nanophotonics **12**(5), 925–935 (2022).
19. K. Sozos, A. Bogris, P. Bienstman, *et al.*, "High-speed photonic neuromorphic computing using recurrent optical spectrum slicing neural networks," Commun. Eng. **1**(1), 24 (2022).
20. M. Lyu, W. Shi, and L. Rusch, "Sip-based ssbi cancellation for ofdm," IEEE Photonics J. **11**(5), 1–13 (2019).
21. A. Lugnan, A. Katumba, F. Laporte, *et al.*, "Photonic neuromorphic information processing and reservoir computing," APL Photonics **5**(2), 020901 (2020).
22. C. Ma, J. Lambrecht, F. Laporte, *et al.*, "Comparing different nonlinearities in readout systems for optical neuromorphic computing networks," Sci. Rep. **11**(1), 24152 (2021).
23. "Vpiphotonics: Simulation software and design services," https://www.vpiphotonics.com/index.php. Accessed: 2024-05-24.
24. F. Laporte, J. Dambre, and P. Bienstman, "Photontorch: simulation and optimization of large photonic circuits using the deep learning framework pytorch," in *2019 IEEE Photonics Society Summer Topical Meeting Series (SUM)*, (IEEE, 2019), pp. 1–2.
25. I. Sutskever, J. Martens, G. Dahl, *et al.*, "On the importance of initialization and momentum in deep learning," in *International conference on machine learning*, (PMLR, 2013), pp. 1139–1147.